International Journal of Nanoelectronics and Materials
Volume 13, No. 1, Jan 2020 [101-112]

Performance of Multi-Function Devices Fabricated from La_2O_3-Doped NiO Thin Films

Asmiet Ramizy[1*], Abubaker S. Mohammed[2] Isam M. Ibrahim[3] and M. H. Eisa[4, 5]

[1]*Department of Physics, College of Science, University of Anbar, Anbar, Iraq.*
[2]*Ministry of Education, Direction of Education in AL-Anbar .*
[3]*Department of Physics, College of Science, University of Baghdad, Baghdad, Iraq .*
[4]*Department of Physics College of Science, Sudan University of Science and Technology, Khartoum 11113, Sudan.*
[5]*Department of Physics, College of Sciences, Imam Mohammad Ibn Saud Islamic University (IMSIU), Riyadh 11623, Saudi Arabia.*

Received 18 May 2019, Revised 17 October 2019, Accepted 30 December 2019

ABSTRACT

Multi-function devices fabricated from lanthanum oxide (La_2O_3)-doped NiO thin films at 0, 2, 4, and 6% wt on porous silicon (PS) substrates were prepared by Pulsed Laser Deposition (PLD) method. PS was fabricated using n-type Si with (111) orientation by the photoelectrochemical etching process (ECE) at a constant etching time of 20 minutes and current density of 15 mA/cm^2. X-ray Diffraction (XRD) and AFM results showed uniform morphology and good crystal quality of the synthesized nanostructures. The energy gap (Eg) of NiO is 3.25 eV, and it increased as the doping ratio was increased. Gas sensing and UV-detection were studied respectively. The maximum sensitivity to H_2S gas was observed in the film doped with 6% La_2O_3 at 100ºC and found to be 3500%. The photosensitivity was 66% for NiO/PS and 118% with La_2O_3 doping ratio of 6%. The novelty of this work is to use a very simple and low-cost method Pulsed Laser Deposition (PLD) to growth La_2O_3 doped NiO as compared with other technique which used to fabricate nanostructure that is either very expensive or very time-consuming.

Keywords: Multi-Function Device, Metal Oxide, Rare Earth, Porous Silicon, Pulsed-Laser Deposition.

1. INTRODUCTION

The complex and tunable nature of metal oxides' electrical properties makes them attractive and interesting substances for many applications such as optoelectronics, solar cells, gas sensors, photodetector, spintronics, and photonic devices [1, 2]. The physical and chemical features of metal oxide nanoparticles are peculiar because they are small in size and have a high density of corner or edge surface sites [3]. Recently, many metal oxide nanostructures have been prepared such as NiO, ZnO, CuO, and Ga_2O_3 [4]. Nickel oxide (NiO) is a normal wide energy band gap semiconductor of about 3.4 to 4.3 eV and p-type conductivity associated with nonstoichiometric deficiencies, including Ni vacancies and O interstitials. Moreover, it is well-known that NiO is stable chemically because of its stable cubic structure and its weak absorption bands in the visible wavelength range as a result of d-d band transitions [5]. These materials have attracted attention by virtue of their excellent chemical stability, low cost, and promising storage properties [6,7]. Some applications of metal oxide NiO films include counter electrodes, gas sensors, displays, LEDs, and variable reactance mirrors [8]. In addition, they are

---

[*]Corresponding Author: *asmat_hadithi@uoanbar.edu.iq*

utilised in catalysts, electrochromic devices, solar cells, battery cathodes, large span optical densities, full cells, and TCOs [9–11]. Such films were elaborately utilised in various deposition techniques: Pulsed Laser Deposition (PLD) [12,13], spray pyrolysis [14], sputtering [15], sol-gel [16], and thermal evaporation [17]. Lanthanum (La) is one of the RE elements which belongs to the lanthanide series. Lanthanum oxide (La_2O3) has electronic and chemical properties which met the requirements for different applications in various field such as electrode materials for fuel cell, gas sensor, and photodetector [18,19]. The PLD method is a multipurpose method, and it is mainly utilised as a result of the stoichiometric transfer between the target and deposition film, thus, it has a lot of advantages. Particularly, it can efficiently control the composition of thin films to simplify their rapid and effective growth process. It makes deposition of oxides, polymers, carbides, nitrides, and metallic systems possible [20]. The aim of this work is to investigate the influence of the rare-earth compound La_2O_3 on the properties of NiO/PS nanofilms prepared by the PLD method at room temperature.

2. MATERIAL AND METHODS

Figure 1 shows the schematic diagram of the fabricated NiO/PS heterojunction. The formation of PS layers was obtained by the electrochemical etching (ECE) of n-type <111> oriented silicon substrate at the resistivity of 1–4 Ω.cm. The ECE cell composed of Teflon (or any polymer that has a high resistance to acid). Si wafer was cut into pieces of square shape (1 cm^2) and anodized in a solution containing 48% HF and ethanol at a ratio of 1:4 and current density of 15 mA/cm^2 for 20 minutes under illumination (70 W halogen lamp situated 20 cm from the sample). Silicon wafers were cleaned ultrasonically in distilled water and acetone. A two-electrode setup was implemented; the anode was Si, and the cathode was Pt mesh. NiO powders with different doping concentrations of La_2O_3 (at 0, 2, 4 and 6% wt) were mixed using a gate mortar and then pressed under 5 tonnes to form targets with 2 cm diameter and 0.2 cm thickness. The targets were ensured dense and homogeneous as much as possible to produce good quality La_2O_3:NiO thin films, which would be deposited by the PLD technique. Film deposition was carried out inside a 10^{-3} Torr evacuated vacuum chamber.

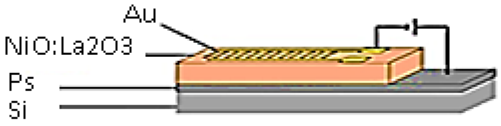

Figure 1. The schematic diagram of NiO:La_2O_3/PS heterojunction.

The focused Q-switched Nd:YAG laser beam was incident at an angle of 45° on the target surface, and the energy of the laser was 500 mJ. Metallization of samples was employed to fabricate the MSM device, and the metal contacts of finger-shaped gold (Au) electrodes of 250 nm thicknesses were deposited on top of the NiO:La_2O_3/PS sample. Au gold pieces were utilized for making Schottky and heterojunction contact with purity 99%, which placed in a boat of tungsten inside the thermal evaporation vacuum system under a high vacuum of 10^{-6} mbar by rotary and diffusion pump. A metal mask consists of interdigitated contact (electrode) with a finger width of 230 µm, finger spacing of 400 µm, and the length of each electrode is about 3.3 mm. Each electrode has four fingers. The Filmetrics F20 was used to determine thin film thickness in the range of 200 ± 5 nm. The structure properties, including crystal size and crystal structure, were studied by an X-ray Diffraction (XRD) system (BRUKER AXS), whose source of radiation was Cu (kα) and the wavelength was 1.5406 Aº. The morphology of the surfaces of the films was tested via AFM, SPM model AA3000, and the FESEM type (FEI Verios 460L) of Supra 50VP device. The photoluminescence spectra were measured by the PL device type (SL 174 - ELICO) of spectrofluorometer, with 150 watts Xenon Arc lamp and excitation and emission from 200-900 nm. Laptop PC and a "PC-interfaced digital multimeter of type UNI-T UT81B" were utilized to register the change in the sensor resistance when exposed to the air-H_2S gas mixing ratio. The spectral response of the detector was measured using a detector test system type infrared spectroradiometer, Model 746.

3. RESULT AND DISCUSSION

3.1 Structure

XRD patterns of the nickel oxide films doped with different concentrations (0, 2, 4 and 6%) of La_2O_3 thin films prepared on PS by PLD at room temperature are given in Figure 2**.** Note that all films are polycrystalline, and the XRD patterns indicate two diffraction peaks, which refer to the formation of nickel oxide with planes of (111) and (200). The films were crystallized in cubic symmetry according to [21]. For the doping ratio of 2%, the increase in the intensity of the diffraction peaks of NiO with increasing doping concentration was noted as well as the appearance of one weak peak with plane (101) at a diffraction angle (2θ) equal to 29.831°, which belongs to La_2O_3 with a hexagonal phase structure according to JCPDS card (No.96-410-2406).

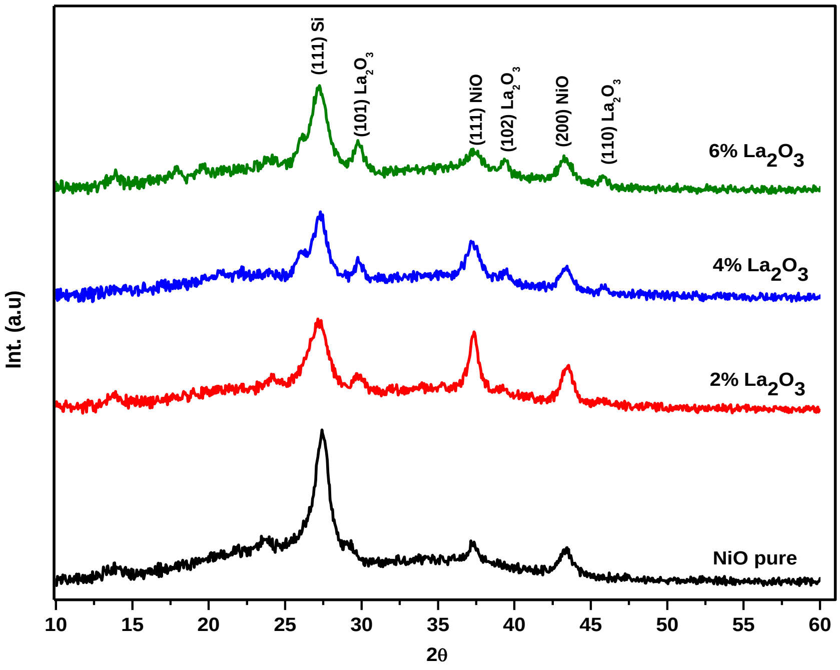

Figure 2. XRD patterns of La_2O_3-doped NiO \ PS at (0, 2, 4, and 6) wt%.

The XRD intensities of La_2O_3 peaks increased with increased doping, which could be as a result of the interaction between La_2O_3 and NiO, and the atoms of the dopant material that take a position in the crystalline lattice of NiO. The two peaks refer to La_2O_3 at rate 4% and 5% respectively at 2θ equal to 39.38 and 45.821 with planes (102) and (110) respectively, according to JCPDS card (No. 96-410-2406). The doping ratios did not change the direction of crystalline growth for the dominant planes, and growth continued towards (111) direction, which refers to the drift competitive growth model, called "the model of the survival of the fastest-growing crystallites" [22]. Drift was supposed so the process of nucleation takes many directions at the beginning of the growth of films and then begins to compete through growth, and the fastest-nuclei continue growing while the other nucleus stops growing [23]. The result showed that the mean crystallite size of NiO decreases when the doping ratio and FWHM are increased; this is illustrated in Table 1.

Table 1 Structural parameters of La_2O_3-doped NiO /PS at (0, 2, 4, and 6) wt%

La_2O_3 %	**2θ (Deg.)**	**FWHM (Deg.)**	**d_{hkl} Exp.(Å)**	**G.S (nm)**	**hkl**	**d_{hkl} Std.(Å)**	**Phase**	**Card No.**
0	27.4520	0.8818	3.2464	9.3	(111)	3.1414	Cub. Si	96-901-3105
	37.3200	0.6446	2.4076	13.0	(111)	2.4066	Cub. NiO	96-900-8694
	43.3800	0.9829	2.0842	8.7	(200)	2.0842	Cub. NiO	96-900-8694
2	27.3520	0.9640	3.2580	8.5	(111)	3.1414	Cub. Si	96-901-3105
	29.8310	0.7140	2.9927	11.5	(101)	2.9921	Hex. La_2O_3	96-410-2406
	37.3160	0.7730	2.4078	10.9	(111)	2.4066	Cub. NiO	96-900-8694
	43.4550	0.8630	2.0808	9.9	(200)	2.0842	Cub. NiO	96-900-8694
4	27.3310	0.9210	3.2605	8.9	(111)	3.1414	Cub. Si	96-901-3105
	29.8230	0.7320	2.9935	11.2	(101)	2.9921	Hex. La_2O_3	96-410-2406
	37.2940	0.9910	2.4092	8.5	(111)	2.4066	Cub. NiO	96-900-8694
	39.3870	0.5320	2.2858	15.9	(102)	2.2862	Hex. La_2O_3	96-410-2406
	43.3710	0.8750	2.0846	9.8	(200)	2.0842	Cub. NiO	96-900-8694
6	27.3170	1.1300	3.2621	7.2	(111)	3.1414	Cub. Si	96-901-3105
	29.8150	0.7220	2.9943	11.4	(101)	2.9921	Hex. La_2O_3	96-410-2406
	37.3720	1.1150	2.4043	7.5	(111)	2.4066	Cub. NiO	96-900-8694
	39.3782	0.5570	2.2863	15.2	(102)	2.2862	Hex. La_2O_3	96-410-2406
	43.3450	1.1320	2.0858	7.6	(200)	2.0842	Cub. NiO	96-900-8694
	45.8211	0.5410	1.9787	15.9	(110)	1.9785	Hex. La_2O_3	96-410-2406

3.2 AFM Morphology

The AFM images for pure NiO thin films with various doping rates of La_2O_3 (0, 2, 4, and 6 % wt) deposited on a glass substrate are shown in Figure 3. Roughness, average diameter, RMS, and surface thickness of samples are illustrated in Table 2. AFM analysis of pure NiO film showed good uniformity, indicating uniform growth for the films. The average diameter increased with increasing doping ratio of La_2O_3. This is contrary to the behaviour of the samples in the results of XRD because XRD differs from AFM. XRD determines crystallite size and penetrates inside the structure, while AFM determines grain size at the surface. The average roughness was increased at 2% doping ratio and then decreased when the doping ratio was increased to 4% and 6%, which could be because of the increase in roughness attributed to grain growth and structure densification of the deposition processes. The increase in roughness is as a result of the presence of numerous hillocks that are faceted and distributed randomly. This is in agreement with [24].

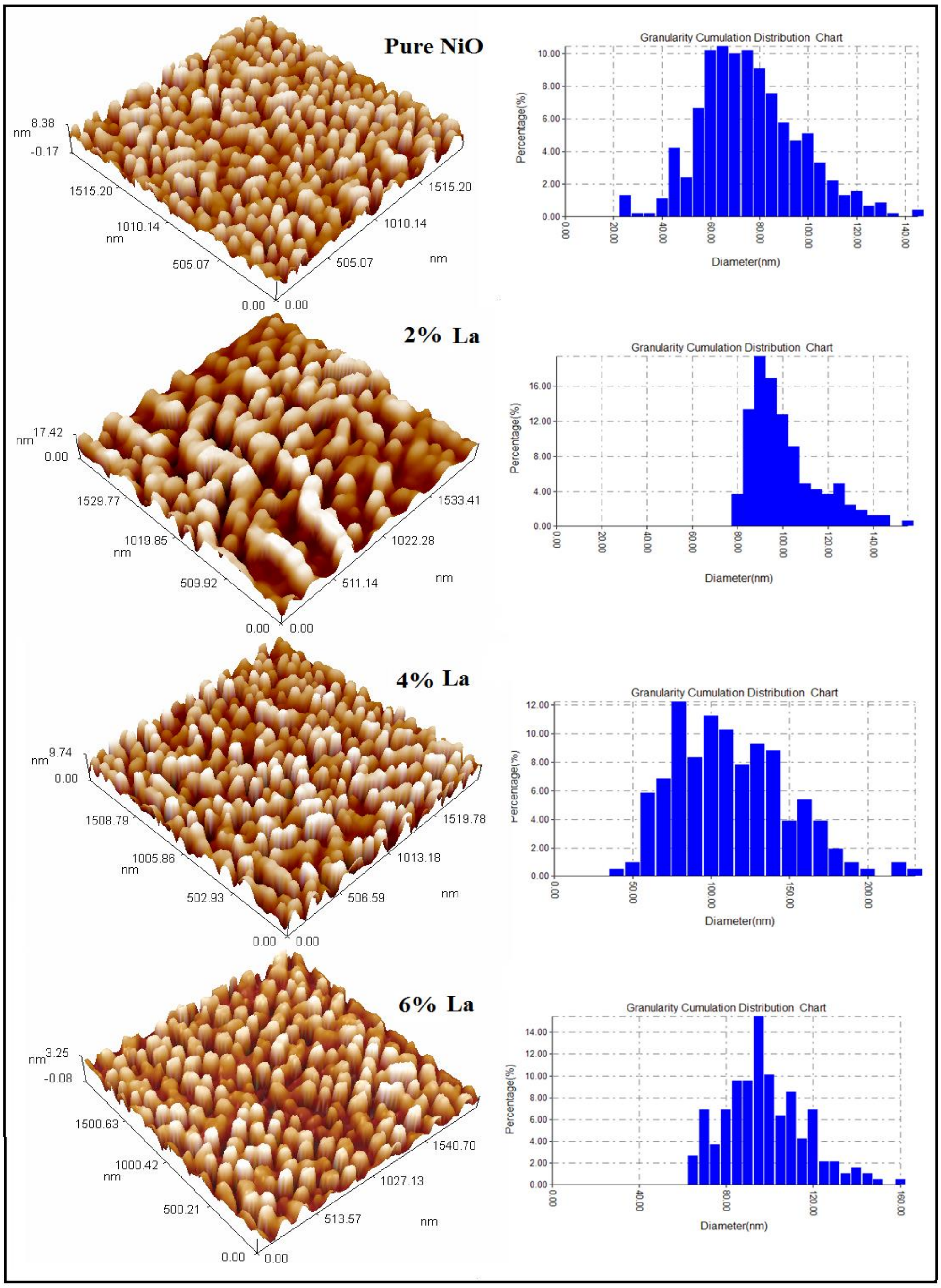

Figure 3. 3-D AFM micrographs of La_2O_3-doped NiO films at doping ratios of 0, 2, 4, and 6%wt.

Table 2 AFM parameters of La_2O_3-doped NiO films at doping ratios of 0, 2, 4, and 6 wt%

Sample	Ave. diameter (nm)	Roughness (nm)	RMS (nm)	Surface thickness (nm)
Pure NiO	73.56	1.62	1.94	8.38
2%La_2O_3	99.0	3.84	4.52	17.42
4% La_2O_3	98.36	2.19	2.58	9.74
6%La_2O_3	95.41	2.0	0.812	3.25

3.3 FESEM

Figure 4 depicts the FESEM images of the surface structure of pure NiO and those doped with lanthanum at 0, 2, and 6% wt on the porous substrate at 15 mA etching current and 20 minutes. Figure (4a) shows the top view of the synthesis of NiO thin film. These images reveal the filling of NiO into the pores of the porous substrate with some places not fully filled. Figure (4b) shows the surface of NiO:La_2O_3/PS at 2% doping ratio. The image illustrates that the deposition of nickel oxide spans the whole Si nanocrystalline, which leads to a general increase in their sizes [25]. This result agrees with the result obtained in AFM and the penetration of NiO:La_2O_3 into the pores. The morphology and size of the NiO nanostructures may influence their electronic, magnetic, optical, and catalytic properties [26]. Figure (4c) shows the morphology of NiO:La_2O_3 at 6% doping ratio. The image appears as a loosely packed network assembled by spherical particles like nano-reef structure. With the decrease in diameter as a result of an increase in La concentration, the presence of voids could be as a result of reduced particle diameters that do not fully fill the pores spaces.

3.4 Photoluminescence Spectroscopy (PL)

The PL spectra for NiO doped with La_2O_3 on silicon substrate by pulsed laser deposition is illustrated in Figure 5. The PL peak position of NiO is blue-shifted as a function of the doping ratio. According to the quantum confinement model, the peak shift is due to increased energy gap (Eg) within the NiO structure. The result also suggests that the bandgap energy (Eg) increased from 3.26 eV to 3.30, 3.36, and 3.41 eV when the doping ratio increased from 0 to 2, 4, and 6% wt, respectively. This is as a result of the reduction to nanosize which supports charge carrier quantum confinement.

3.5 Gas Sensing

In this study, the sensing properties of NiO films with 0, 2, and 6% of lanthanum deposited on the PS at etching current of 15 mA and constant time of 20 minutes for H_2S gas are investigated as a function of time and operating temperature. Figure 6 shows the resistance of the pure NiO/PS substrate as a function of time with on/off gas valve exposed to 3% concentration of H_2S gas at RT of 50 and 100ºC, respectively. The result showed that the resistance value decreased when the gas valve was off (Gas off) and increased when the gas valve was on (Gas on) [27]. The sensitivity versus the operating temperature for NiO:La_2O_3 films at 2 and 6% ratios for H_2S gas are demonstrated in Figures 7 and Figure 8. These figures show an increase in sensitivity with increasing doping ratio and temperature operation. The catalyst effect of La_2O_3 nanoparticles in the structure of metal oxide. These new structures increased sensitivity of NiO by decreasing the energy needed for splitting H_2 or O_2 molecules on the surface of NiO. The result showed the increase in sensitivity with increasing temperature operators, this is a natural result because the conductivity of semiconductors increases with high temperatures. It was observed that the optimal temperature was 100°C. The maximum sensitivity to H_2S gas was observed when the film was doped with 6% La_2O_3 at 100ºC and found to be 3500%, as shown in the results listed in Table 3. These results indicate that lanthanum is a good material for the detection of H_2S gas.

Table 3 Sensitivity, Response time and recovery time of undoped NiO/PS doped with La_2O_3 at (0, 2 and 6% wt)

Sample		**Response time (s)**			**Recovery time (s)**			**Sensitivity %**		
		RT	50	100	RT	50	100	RT	50	100
Pure		13.5	10	14.4	18	16	16.2	106.5	88.4	40
2%La_2O_3		2.0	4.5	2.1	2.2	1.8	2.7	108.3	170.2	187.4
6%La_2O_3		1.8	2	1.8	2.7	4.5	2.2	248.1	300	3519

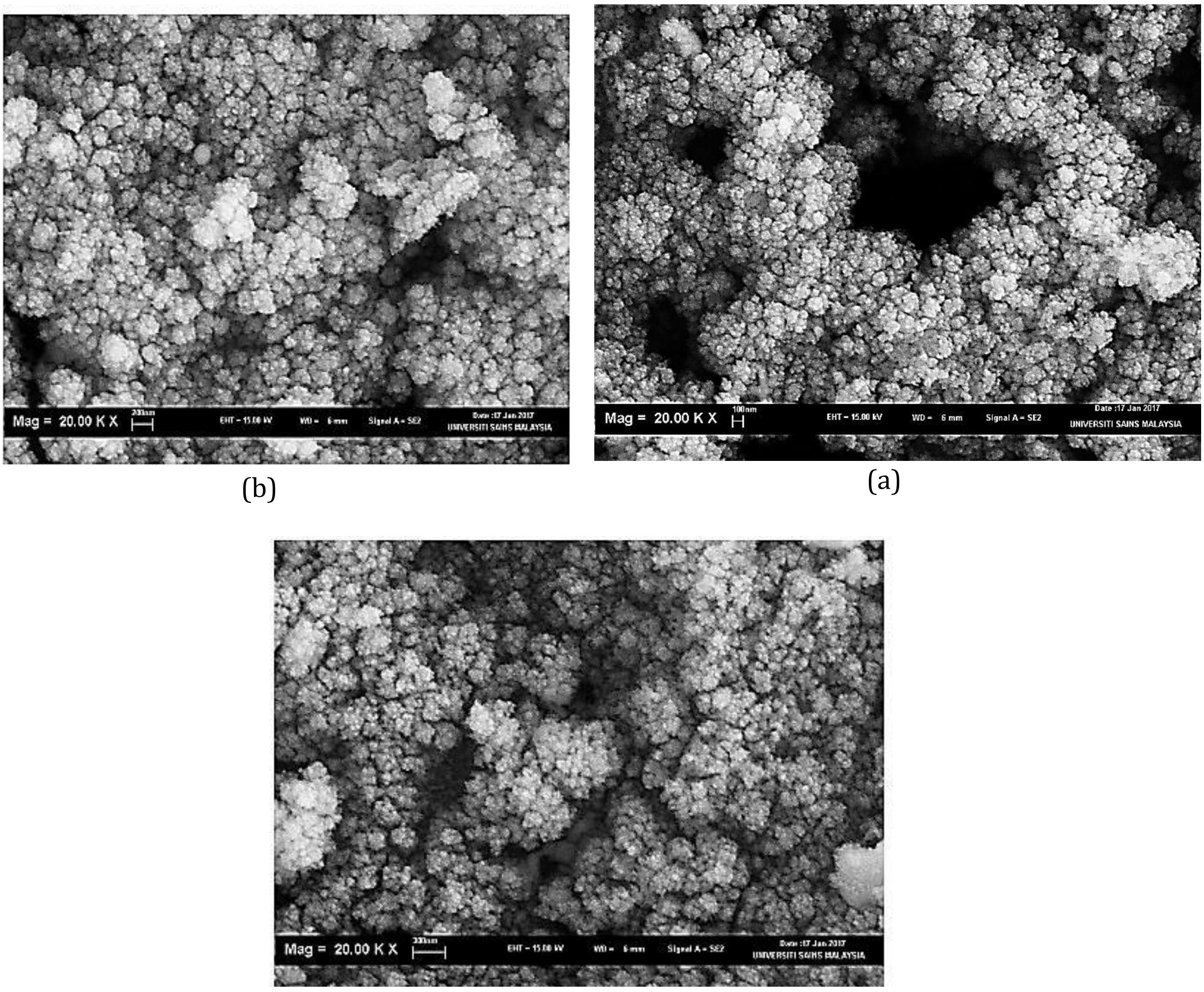

(b) (a)

(c)

Figure 4. FE-SEM images of (a) NiO/PS, (b) NiO: La_2O_3/PS at 2%, and (c) NiO:La_2O_3/PS at 6%.

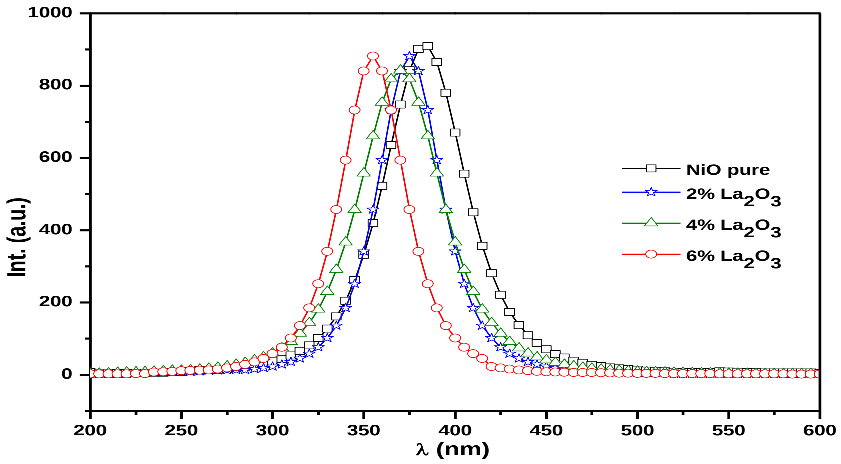

Figure 5. Photoluminescence spectra of NiO: La_2O_3 at (0, 2, 4, 6%).

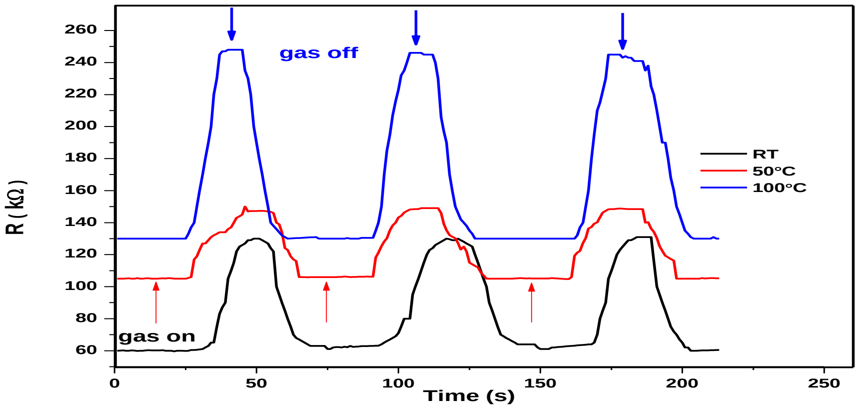

Figure 6. Resistance of Au/NiO /PS as a function of time for H_2S gas.

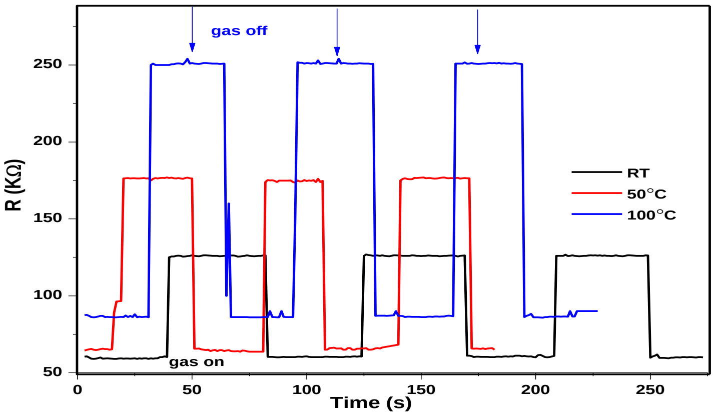

Figure 7. Resistance of Au/NiO: La_2O_3/PS at 2% as a function of time for H_2S gas.

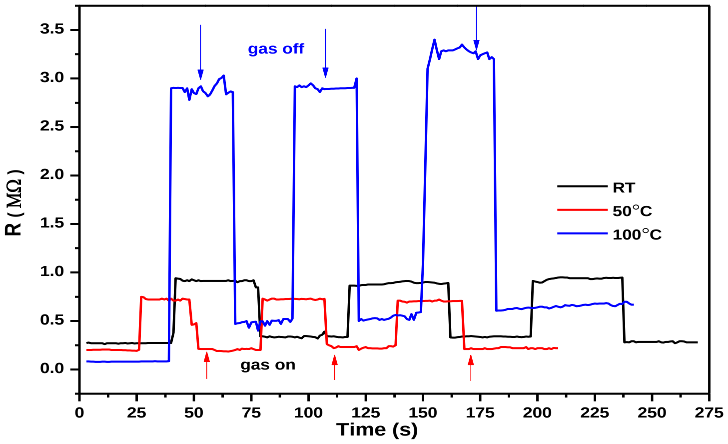

Figure 8. Resistance of Au/NiO:La_2O_3/PS at 6% as a function of time for H_2S gas.

3.6 Photosensitivity (S)

The repeatability of the prepared Au/NiO:RE/PS MSM PD was examined by testing the photoresponse. The light sensitivity was measured by illuminating the photodetector with UV light with a wavelength of 360 nm at 7 W/cm^2. Figure 9 shows the repetitive switching (on-off) of the blue light for the fabricated PDs of Au/NiO:La_2O_3/PS. This sample has photosensitivity of 66%; for NiO/PS, with increased La_2O_3 doping, the sensitivity increased to 118%. Table 4 shows the photosensitivity, rise time, and recovery time. Notably, doping with rare earth elements leads to PD improvement, which can be attributed to the increasing rare earth concentration.

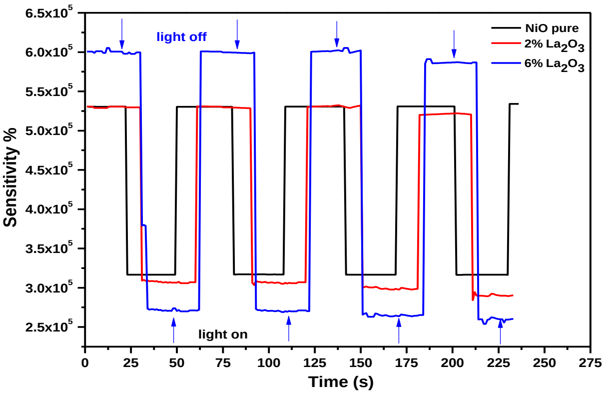

Figure 9. Repetitive switching of the Au/NiO: La_2O_3/PS PD under (UV)365 nm at 0, 2% and 6%.

Table 4 Photoconductivity parameters of Au/NiO: La_2O_3/PS at 0, 2 and 6% ratio

Sample	Sensitivity (S)%	Rise Time (s)	Recovery Time (s)
NiO/PS	66	0.800	0.800
2%La_2O_3/PS	72.2	0.815	0.811
6%La_2O_3/PS	118	0.814	0.805

3.7 Spectral Responsiveness

Figure 10 shows the change in response as a function of the wavelength at the reverse bias voltage (1 volt) of the Au/NiO:La_2O_3/PS at 0, 2, and 6% wt. The spectral response was increased by increasing the wavelength of the incident rays to about 360-320 nm. Two peaks of spectral response were observed, the first at a wavelength of 360 nm, the cutting length of the NiO film, and the second at a wavelength of 760 nm returned to porous silicon; these correspond to [28]. The increase in responsiveness with an increase in wavelength within the range of 300-380 nm in the ultraviolet and near-visible area is due to the absorption of short wavelengths at the surface of the NiO film, which has a large absorption coefficient at those lengths. The measured values of responsiveness are, 0.11, 0.12, and 0.151 A/W at 360, 330 and 320 nm at doping ratios 0, 2 and 6% wt respectively.

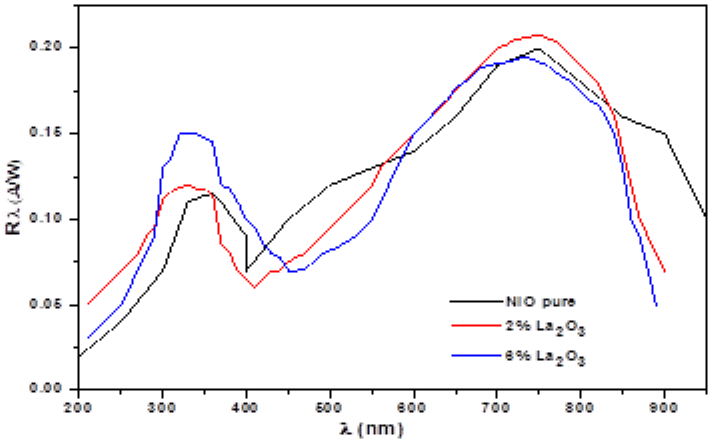

Figure 10. Response spectrum of the Au/NiO:La_2O_3/PS at 0%, 2% and 6%.

4. CONCLUSION

The effects of La_2O_3 doping ratios on the performance of fabricated NiO/PS multi-function devices were examined. XRD pattern showed that NiO films were crystallized in cubic symmetry, and hexagonal phase structure returned to lanthanum oxide. AFM images of NiO doped with La_2O_3 showed a change in average diameter with increasing doping ratio. The energy gap (Eg) increased as the doping ratio increased. Gas sensing, UV detection, and spectral responsiveness were studied as the multi-functions.

ACKNOWLEDGEMENT

This research did not receive any specific grant from funding agencies in the public, commercial, or not-for-profit sectors.

REFERENCE

[1] P. Shankar, J. B. B. Rayappan, Sci. Jet., **4**, 126 (2015) 1-18.
[2] J. Wu, J. Cao, W-Q. Han, A. Janotti, H.-C. Kim, Springer, New York, (2012).
[3] P. Ayyub, V. R. Palkar, S. Chattopadhyay & M. Multani, Phys. Rev. B: Condens Matter **51**, 9 (1995) 6135-6138.
[4] G. N. Dar, PhD thesis, Patras. Greece, (2015).
[5] B. Parida, S. Kim, M. Oh, S. Jung, M. Baek, J. R you, H. Kim, Mater. Sci. Semicond. Process. **71** (2017) 29–34.
[6] D. S. Jbaier, J. A. Simon, K. S. Khashan, Eng. & Tech. J. **33,** 5 (2015) 951-959.
[7] A. F. Saleh, IJAIEM **2**, 1 (2013) 16-21.
[8] M. Guziewicz, W. Jung, J. Grochowski, M. Borysiewicz, K. Golaszewska, R. Kruszkaa, A. Baranska, A. Piotrowska, B.S. Witkowskib, J.Z. Domagala, M. Gryzinski, K. Tyminska and A. Stonert, Acta Phys. Pol., A **120,** 6A (2011) 69-722.

[9] M. Guziewics, J. Grochowski, M. Borysiewicz, E. Aminska, J. Domagala, W. Rzodkiewicz, B. Witkowski, K. Golaszewska, R. Kruszka, M. Ekielski & A. Piotrowski, Opt. Appl., **XLI** (2), (2011) 431-440.
[10] A. S. Devasthali & S. G. Kandalkar, IOSR-JCE **17**(2015) 47-51.
[11] D. Wang, R. Xu, X. Wang & Y. Li, Nanotechnology **17**, 4 (2006) 979–983.
[12] A. I. Hassan, K. S. Khashan, J. A. Saimon, Eng. &Tech. J. **33**, 1 (2015) 52-60.
[13] H. S. Tareq, Eng. &Tech. J **32**, 3 (2014) 444- 452.
[14] M. Abdnabi, Indian J. Appl. Res. **4**, 10 (2014) 533-537.
[15] E. A vendano, L. Berggren, G. A. Niklasson, C. G. Granqvist & A. Azens, Thin Solid Films, **496**, 1 (2006) 30-36.
[16] M. Alagiri, S. Ponnusamy, C. Muthamizhchelvan, J. Mater. Sci.-Mater. Electron. **23**, 3 (2012) 728–732.
[17] J. M. Choi, S. Im, Appl. Surf. Sci. **244**, 1-4 (2005) 435–438.
[18] W. M. White, "Encyclopedia of Geochemistry", Handbook Springer, (2014).
[19] M. Ibrahim, A. Ramizy, A. S. Mohammed," Rare Earth Doped NiO Nanostructure for H2S Sensor and photodetector"., LAP LAMPERT ACADEMIC PUBLISHING, (2018).
[20] A. Largeanu, G.O. Pompilian, D.G. Galusca, M. Ago and S.Gurlui, U.P.B. Sci. Bull., Series A **73** (3) 195- 202 (2011).
[21] M. Ibrahim, A. S. Mohammed, A. Ramizy, J. of Ovonic Research, **14**, 1 (2018) 17–25.
[22] A. V. Drift, Philips Res. Repts, **22** (1967) 267–288.
[23] G. Li, X. Zhu, X. Tang, W. Song, Z. Yang, J. Dai, Y. Sun, X. Pan & S. Dai, J. Alloys Compd. **509**, 14 (2011) 4816-4823.
[24] X. Q. Pan & L. Fu, J. Electroceram. **7**, 1 (2001) 35-46.
[25] R. Riahi, L. Derbali, B. Ouertaniand H. Ezzaouia, Appl. Surf. Sci. **341,** 1-21 (2017).
[26] B. Zhao, X.K. Ke, J.H. Bao, C. L. Wang, L. Dong ,Y.W. Chen & H.L. Chen, J. Phys. Chem. **113**, C (2009) 14440-14447.
[27] T. Akamatsu, T. Itoh, N. Izu & W. Shin, Sensors **13**, 9 (2013) 12467–12481.
[28] B. E. B. Al-Jumaili, Z. A. Talib, A. Ramizy, N. M. Ahmed, L. Y. Josephine, S. B. Paiman, I. B. Muhd, and S. A. Abdulateef, J Nanomater, (2016) 1-8.